

Important role of magnetization precession angle measurement in inverse spin Hall effect induced by spin pumping

Surbhi Gupta^{1,a)}, Rohit Medwal¹, Daichi Kodama¹, Kouta Kondou², YoshiChika Otani^{2,3}, Yasuhiro Fukuma^{1,2,a)}

¹*Department of Computer Science and Electronics, Kyushu Institute of Technology, Iizuka, Fukuoka 820-8502, Japan*

²*Center for Emergent Matter Science, RIKEN, 2-1 Hirosawa, Wako 351-0198, Japan*

³*Institute for Solid State Physics, University of Tokyo, Kashiwa 277-8581, Japan*

Abstract

Here, we investigate spin Hall angle of Pt in Ni₈₀Fe₂₀/Pt bilayer system by using a broadband spin pumping and inverse spin Hall effect measurement. An out-of-plane excitation geometry with application of external magnetic field perpendicular to the charge current direction is utilized in order to suppress unwanted galvanomagnetic effects. Magnetization precession angle (θ_c) on ferromagnetic resonance for wide excitation frequency range (4-14 GHz) is estimated from the rectification voltage of anisotropic magnetoresistance (AMR) and a conventional method of using microwave power in a coplanar waveguide. A marked difference in θ_c profiles for the different methods is observed, resulting in the large variation in estimated values of spin current density at Ni₈₀Fe₂₀/Pt interface. The frequency dependence of the spin current density estimated using AMR effect is found to be similar to that of the inverse spin Hall voltage. We obtain the frequency-invariant spin Hall angle of 0.067 ± 0.002 .

^{a)} Electronic mail: sgupta@fukuma-lab.info, fukuma@cse.kyutech.ac.jp

Over the past decades large number of experimental as well as theoretical attempts have been made to construct new insights and applications of spin pumping (SP) effect since Tserkovnyak, *et al.* theoretically proposed the SP effect to inject pure spin current (J_s) from a precessing ferromagnetic metal (FM) to neighboring normal metal (NM).¹ Indeed, SP effect driven by its versatility is being widely explored to determine spin to charge current conversion efficiency, referred as spin Hall angle (Θ_{SH}), in various kind of materials ranging from strong spin-orbit coupling system of heavy metals²⁻³, conventional semiconductors like (Si and Ge)⁴⁻⁵, wide-band gap semiconductor oxides (ZnO, ITO)⁶⁻⁷ to ferromagnetic metallic alloys^{3,8} oxides like SrRuO₃⁹ and even organic polymers¹⁰. In practice, other techniques of non-local injection in lateral spin valve structure¹¹, spin-torque ferromagnetic resonance¹²⁻¹⁴ and time-resolved magneto-optical Kerr effect¹⁵ have also been established by various groups to measure Θ_{SH} of different materials. However very recent reports of significant modification in SP efficiency by further introducing complex interfacial effects¹⁶⁻¹⁷ and novel application of SP effect to probe magnetic phase transitions in antiferromagnetic systems¹⁸⁻¹⁹ undoubtedly highlight that it is a subject of intensive research with enormous possibilities.

In a prototypical setup of spin pumping-inverse spin Hall effect (SP-ISHE) measurement, SP occurs during the excitation of ferromagnetic resonance (FMR) when precession of magnetization in FM injects pure spin current into adjacent NM layer and then the injected spin current is converted into the transverse dc voltage by means of ISHE in NM. Generally in SP-ISHE measurement set-up, other Galvanomagnetic effects such as anisotropic magnetoresistance (AMR), planar Hall effect and anomalous Hall effect also generate spurious dc voltage signal because of capacitive and/or inductive coupled microwave current in the FM/NM sample.²⁰ Most of the previously reported studies assumed that purely Lorentz line shape of the voltage signal

originates from ISHE contribution whereas antisymmetric line shape corresponds to that from the unwanted rectification signals. However, this assumption holds true only for specially designed device configuration and for particular microwave frequencies, as clearly demonstrated by Harder et al.²¹ and Obstbaum et al.²² Therefore, systematic and controlled studies of line shape analysis in different external magnetic field direction were performed in order to carefully distinguish ISHE induced dc voltage (V_{ISHE}) unambiguously from unwanted spurious signal.²²⁻²⁶

However, in such studies, precession of the magnetization at FMR, i.e., the magnetization precession angle (θ_c) and its trajectory²⁶⁻²⁷ is not sufficiently characterized. It is important to estimate independently the precession angle (θ_c) to have quantitative analysis of Θ_{SH} as $\Theta_{\text{SH}} \propto V_{\text{ISHE}} / J_s$, where J_s is being second order effect in the precession angle ($\sin^2 \theta_c$). Moreover, waveguide based experimental set-up shows different microwave power losses and in-turn varying θ_c values in the range of sweeping frequencies. Therefore these parameters should be characterized in such measurement scheme separately. Otherwise large disparity may happen in estimated values, which had already led to large inconsistency in Θ_{SH} value of the most studied metal Pt varying from 0.0067 to 0.11 and dubious frequency dependent behavior in spite of employing same method of the SP-ISHE measurement.²⁸ In this letter, we demonstrate the precise estimation of Θ_{SH} by independently evaluation of θ_c in each input microwave frequency. In order to determine the amplitude of J_s caused by SP, the different evaluation methods, namely microwave magnetic field (h_{rf}) evaluation using input setting power (P_{input})²⁹⁻³⁰, transmitted power (P_{trans})³¹ and absorbed power (P_{ab})^{7,32} measurements and a direct evaluation of θ_c by using rectified dc voltage due to AMR effect³³⁻³⁴, are compared to quantify frequency dependent θ_c in broad range of microwave frequency 4-14 GHz. In addition, out-of-plane microwave excitation geometry is opted for both θ_c and SP-ISHE measurements in the Py/Pt bilayer to completely

avoid spurious rectification voltage signals. We observed similar behavior of J_s estimated from the rectification voltage due to AMR and V_{ISHE} as a function of applied microwave frequency, which provided reliable and invariant value of Θ_{SH} in the frequency range. On the other hand, Θ_{SH} deduced from J_s determined from the P_{input} , P_{trans} and P_{ab} measurements showed significant variation.

Figure 1(a) and 1(b) show optical top-view images of two distinct devices designed to measure θ_c using AMR induced rectification voltage in Py (10 nm) layer and V_{ISHE} in Py (10 nm)/Pt (10 nm) bilayer, respectively. In both devices, micro-strip with lateral dimensions of $300 \times 5 \mu\text{m}^2$ is fabricated using photolithography process. Coplanar waveguide (CPW) structure of Ti (5 nm)/Au(200 nm) was deposited such a way that Py and Py/Pt micro-strip lied in the space between ground and central signal line for inducing FMR in Py with out-of-plane microwave field (h_{rf}) as shown in Fig. 1(c). In addition lock-in-technique was employed to improve signal-to-noise ratio and therefore amplitude modulated microwaves referenced at 79 Hz were applied to CPW using a signal generator. For θ_c measurement using AMR, an additional dc current (I_{dc}) ranging from 0.1 to 0.5 mA was applied (Fig. 1(a)). Then lock-in-amplifier picked up the voltage signal as a function of sweeping external magnetic field H_{dc} which can be rotated in-plane ($0 \leq \beta \leq 360^\circ$) where β is defined as angle of H_{dc} with respect to the micro-strip (Fig. 1(c)). In-plane H_{dc} field was applied parallel to the Py micro-strip ($\beta = 0$) in the θ_c measurement because its geometry then became sensitive to the modulation driven by oscillating resistance of Py. During V_{ISHE} measurement, H_{dc} was applied perpendicular to the strip ($\beta = 90^\circ$).

Figure 2(a) shows dc voltage spectra for $I_{\text{dc}} = 0.4$ mA as a function of H_{dc} for different applied microwave frequency ranging from 4 to 14 GHz, in the step size of 1 GHz with P_{input} of 15 dBm. We chose high microwave signal of 15 dBm to compensate the transmission losses at

multiple stages of microwave cable, connectors and probe station in the present setup. The detected spectrum showed complex line shape signal around the resonance field (H_r) for all the applied frequency range. The amplitude of the spectra (V_θ) showed an expected decrease with increasing frequency because a torque that pulls the magnetization back into equilibrium condition increases with increasing H_{dc} and therefore θ_C decreases.³⁴ The inset of Fig. 2(a) shows V_θ measured as a function of input microwave power (P_{input}) ranging from 13 to 18 dBm at fixed frequency of $f = 7$ GHz and $I_{dc} = 0.3$ mA. As microwave field amplitude (h_{rf}) increases as a square root of applied power and θ_C increases linearly with h_{rf} field, the linear scaling of V_θ with microwave power with intercept at origin (0,0) shown in the inset is found to be consistent with the theory, implying that the present experiment was performed in a linear excitation regime.²⁰ The frequency-dependent behavior of θ_C was estimated using following equation^{3, 33-34},

$$\theta_C = \sin^{-1}(\text{sqrt}(V_\theta/I_{dc} \times \Delta R_{AMR})) , \quad (1)$$

where $\Delta R_{AMR} = R_{\parallel} - R_{\perp}$ is the maximum change in dc magnetoresistance and R_{\parallel} and R_{\perp} are resistance of the Py micro-strip in the saturated state when H_{dc} is applied parallel and transverse to the applied current direction, respectively. An AMR ratio ($\Delta R_{AMR}/R_{\parallel}$) of approximately 0.5% was determined for Py using four probe method. Figure 2(b) depicts θ_C in Py as a function of applied microwave frequency obtained from the AMR and microwave power measurements. The microwave field h_{rf} was estimated using Ampere's Law, $h_{rf} = \frac{\mu_0 \sqrt{P/Z}}{2\pi w} \ln(1 + \frac{w}{D})$ where w is the width (10 μm) of the signal line in CPW and D is the space (5 μm) between the signal line and the Py micro strip, P is the microwave power (P_{input} and P_{trans}) and Z is the characteristic impedance of 50 Ω . Thereafter, frequency dependent θ_C in the limit of a small precession angle was extracted using $\theta_C = h_{rf}/2\Delta H_{Py}$,¹⁶ where ΔH defines the half width of FMR spectra at the half

maximum intensity. We also calculated θ_C using absorbed power (P_{ab}) which is estimated from FMR measurement using VNA^{7,32} while the transmitting power (P_{trans}) is recorded using a power meter. For better understanding, the detail procedure of P_{ab} and P_{trans} measurement is shown in Fig. S1 provided in the supplementary section and frequency dependent behavior of P_{ab} and P_{trans} is also shown in supplementary Fig. S2. A continuous decrease in θ_C as a function of the applied frequency is observed, however, the decreasing behavior is quite different for the measurement methods, which in turn further affect the determination of injected J_s .

To determine J_s and Θ_{SH} , frequency dependent V_{ISHE} as a function of H_{dc} is measured across Py/Pt bilayer micro-strip keeping same input power P_{input} of 15 dBm. To avoid spurious AMR signal (V_{AMR}) from V_{ISHE} , we strictly aligned H_{dc} at $\beta = 90^\circ$ or 270° with respect to micro-strip. Such configuration led to zero V_{AMR} contribution while V_{ISHE} reaches to maximum amplitude as V_{AMR} is proportional to $\sin 2\beta$ whereas V_{ISHE} exhibits $\sin\beta$ dependency in the out-of-plane h_{rf} excitation configuration.^{22,35} Figure 3(a) shows a symmetric Lorentz line shaped V_{ISHE} spectrum as a function of H_{dc} for different excitation frequencies where its sign reversal with equal magnitude under H_r inversion, implies its ISHE origin. In support, the inset in Fig. 3(a) provides magnified view of purely symmetric line shape of detected voltage signal for $f = 10$ GHz where solid symbols depict experimental data while solid line represents the Lorentz fit. Then injected J_s into the Pt layer upon FMR excitation for different applied frequency was calculated using²⁰

$$J_s = \frac{2e}{h} \times \frac{\hbar\omega}{4\pi} g^{\uparrow\downarrow} \sin^2 \theta_C \left[2\omega \frac{\left(\gamma M_S + \sqrt{(\gamma M_S)^2 + (2\omega)^2} \right)}{(\gamma M_S)^2 + (2\omega)^2} \right] \quad (2)$$

where $\omega = 2\pi f$ is the angular frequency, $g^{\uparrow\downarrow}$ is the spin mixing conductance of the Py/Pt interface, $\gamma = g\mu_B/\hbar$ is the gyromagnetic ratio, g is the Lande's factor, μ_B is the Bohr magnetron

and M_S is the saturation magnetization. Frequency independent $g^{\uparrow\downarrow} = 1.9 \times 10^{19} \text{ m}^{-2}$ of Py/Pt interface is estimated using $g^{\uparrow\downarrow} = \frac{\gamma}{\omega} \frac{4\pi M_S t_{PY} \delta}{g\mu_B}$,²⁰ where δ accounts for broadening in line width of the FMR spectra ($\delta = \Delta H_{Py/Pt} - \Delta H_{Py}$) due to loss in angular spin momentum in Py during SP and M_S of 870 mT is determined by fitting the Kittel formula, $\omega = \gamma\mu_0\sqrt{H_r(H_r + 4\pi M_S)}$.²⁰ It is important to mention here that the frequency dependence of θ_C defined in Eq. (2) for Py/Pt is not assumed to be same as precession cone angle θ_C of Py; first we determined the amplitude of h_{rf} in the sample by using $h_{rf} = 2\theta_C \times \Delta H_{Py}$. Next, frequency dependence of θ_C for Py/Pt in the SP measurement configuration with $\beta = 90^\circ$ is deduced from $\theta_C = h_{rf} / 2\Delta H_{Py/Pt}$ because of the same design of both samples for Py and Py/Pt, as can be seen in Fig. 1. Figure 3(b) shows the frequency dependence of J_S estimated from four different θ_C approaches as discussed in the previous paragraph. The behavior estimated from AMR measurement shows initial increment in the magnitude up to the excitation frequency of 10 GHz, followed by a decrease till 14 GHz, which is found to be similar to the experimentally obtained trend of V_{ISHE} as shown in Fig. 3(a). On the other hand, J_S values estimated from the microwave power measurements showed monotonic decrease and/or increase with applied frequency. Note that for $f = 10$ GHz, $J_S \sim 5.8 \times 10^6 \text{ A/m}^2$ is determined from P_{trans} measurement which is roughly one order less than J_S value of $4.4 \times 10^7 \text{ A/m}^2$ obtained from AMR method. Whereas J_S values estimated from P_{input} as well as P_{ab} showed uplift in whole frequency range due to the overestimated values of θ_C as shown in Fig. 2(b). Such a large variation in the estimated values of J_S further resulted into the quite different values of Θ_{SH} for the same Py/Pt sample. As injected J_S converts into dc transverse charge current J_C via ISHE due to high spin orbit coupling in Pt, defined by $J_C = \Theta_{SH} \times J_S$, the resultant voltage V_{ISHE} generated along the Py/Pt sample can be written as²⁰

$$V_{\text{ISHE}} = \Theta_{\text{SH}} J_S \left[\frac{L}{\sigma_{\text{Pt}} t_{\text{Pt}} + \sigma_{\text{Py}} t_{\text{Py}}} \lambda_{\text{sd}} \tanh\left(\frac{t_{\text{Pt}}}{2\lambda_{\text{sd}}}\right) \right] \quad (3)$$

where L is the length of the Py/Pt strip, σ_{Pt} and σ_{Py} are conductivities of Pt and Py layer, t_{Pt} and t_{Py} are their respective thicknesses and λ_{sd} is the spin diffusion length of Pt. Considering $\lambda_{\text{sd}} = 1.2$ nm as previously reported for the sample fabricated in the same conditions¹³ and $\sigma_{\text{Pt}} = 2.5 \times 10^6 \Omega^{-1}\text{m}^{-1}$ and $\sigma_{\text{Py}} = 2.86 \times 10^6 \Omega^{-1}\text{m}^{-1}$ as experimentally measured for present samples, the estimated Θ_{SH} as a function of applied frequency (4-14 GHz) is plotted in Fig. 4. $\Theta_{\text{SH}} \sim 0.067 \pm 0.002$ of Pt using independent measurement of θ_{C} from the AMR method revealed a frequency invariant behavior while Θ_{SH} values determined from P_{trans} showed a continuous and steep increase from 0.02 to 0.33 in the given microwave frequency range. To further emphasize the θ_{C} role, we also plotted Θ_{SH} values determined using P_{input} in the inset of Fig. 4 where underestimated values of Θ_{SH} also showed frequency dependent behavior. Important to mention here that smaller Θ_{SH} values determined from P_{ab} measurement also showed a steady behavior in the frequency range, however, the monotonic increase in J_S values with the microwave frequency in this case was also not consistent with V_{ISHE} . Therefore the experimental data presented above clearly demonstrate that independent AMR measurement of θ_{C} is important, especially for waveguide setup. The utilization of out-of-plane excitation geometry in the Py strip helps into the unambiguous determination of symmetric Lorentzian line shape V_{ISHE} signal. This combined methodology is necessary to obtain frequency invariant Θ_{SH} which is a material specific parameter.

In summary, we investigated the indispensable role of independent estimation of θ_{C} in the analysis of SP-ISHE effect, specifically in case of integrated co-planar waveguide architecture. Direct estimation of θ_{C} using rectified dc voltage due to AMR showed relatively small change in

θ_c magnitude with an increase of applied microwave frequency whereas frequency dependent θ_c behavior estimated from conventional method of employing microwave power showed a monotonic decrease. As a result, estimated values of J_s differed by more than an order of magnitude. Most important, the frequency dependent J_s behavior estimated using the AMR measurement is found to be similar trend to experimentally obtained values of V_{ISHE} amplitude, resulted in the frequency-invariant spin Hall angle ($\Theta_{\text{SH}} \sim 0.067 \pm 0.002$) of Pt for the studied frequency interval of 4-14 GHz. This approach essentially offers a simplified and reliable way to investigate the fundamental parameters of spin Hall effect in new promising materials using SP-ISHE measurements.

Supplementary Material

See supplementary material for complete understanding of the detail procedure of microwave power (P_{ab}) and (P_{trans}) measurement.

Acknowledgement

Financial support from Grant-in-Aid for Encouragement of Young Scientists (Grant No. 16K18079) and Grant-in-Aid for Scientific Research on Innovative Area, “Nano Spin Conversion Science” (Grant No. 26103002) are gratefully acknowledged. This work was partially supported by the Asahi Glass Foundation.

References

1. Y. Tserkovnyak, A. Brataas, and G. E. W. Bauer, *Phys. Rev. Lett.* **88**, 117601 (2002).
2. E. Saitoh, M. Ueda, H. Miyajima, and G. Tatara, *Appl. Phys. Lett.* **88**, 182509 (2006).
3. W. Zhang, M. B. Jungfleisch, W. Jiang, J. Sklenar, F. Y. Fradin, J. E. Pearson, J. B. Ketterson, and A. Hoffmann, *J. Appl. Phys.* **117**, 172610 (2015).
4. K. Ando and E. Saitoh, *Nature Comm.* **3**, 629 (2012).
5. J.-C. Rojas-Sánchez, M. Cubukcu, A. Jain, C. Vergnaud, C. Portemont, C. Ducruet, A. Barski, A. Marty, L. Vila, J.-P. Attané, E. Augendre, G. Desfonds, S. Gambarelli, H. Jaffrès, J.-M. George, and M. Jamet, *Phys. Rev. B* **88**, 064403 (2013).
6. J. -C. Lee, L. -W. Huang, D. -S. Hung, T. -H. Chiang, J. C. A. Huang, J. -Z. Liang, and S. -F. Lee, *Appl. Phys. Lett.* **104**, 052401 (2014).
7. Z. Qiu, T. An, K. Uchida, D. Hou, Y. Shiomi, Y. Fujikawa, and E. Saitoh, *Appl. Phys. Lett.* **103**, 182404 (2013)
8. A. Tsukahara, Y. Ando, Y. Kitamura, H. Emoto, E. Shikoh, M. P. Delmo, T. Shinjo, and M. Shiraishi, *Phys. Rev. B* **89**, 235317 (2014).
9. M. Wahler, N. Homonnay, T. Richter, A. Müller, C. Eisenschmidt, B. Fuhrmann, and G. Schmidt, *Sci. Rep.* **6**, 28727 (2016).
10. D. Sun, K. J. van Schooten, M. Kavand, H. Malissa, C. Zhang, M. Groesbeck, C. Boehme, and Z. V. Vardeny, *Nat. Mater.* **15**, 863 (2016).
11. T. Kimura, Y. Otani, T. Sato, S. Tkahashi, and S. Maekawa *Phys. Rev. Lett.* **98**, 249901 (2007)
12. L. Liu, T. Moriyama, D. C. Ralph, and R. A. Buhrman, *Phys. Rev. Lett.* **106**, 036601 (2011).
13. K. Kondou, H. Sukegawa, S. Mitani, K. Tsukagoshi, and S. Kasai, *Appl. Phys. Exp.* **5**, 073002 (2012).
14. A. Ganguly, K. Kondou, H. Sukegawa, S. Mitani, S. Kasai, Y. Niimi, Y. Otani, and A. Barman, *Appl. Phys. Lett.* **104**, 072405 (2014).
15. A. Ganguly, R. M. Rowan-Robinson, A. Haldar, S. Jaiswal, J. Sinha, A. T. Hindmarch, D. A. Atkinson, and A. Barman, *Appl. Phys. Lett.* **105**, 112409 (2014).
16. T. Nan, S. Emori, C. T. Boone, X. Wang, T. M. Oxholm, J. G. Jones, B. M. Howe, G. J. Brown, and N. X. Sun, *Phys. Rev. B* **91**, 214416 (2015).

17. S. Karube, K. Kondou, and Y. Otani, *Appl. Phys. Exp.* **9**, 033001 (2016).
18. L. Frangou, S. Oyarzún, S. Auffret, L. Vila, S. Gambarelli, and V. Baltz, *Phys. Rev. Lett.* **116**, 077203 (2016).
19. Z. Qiu, J. Li, D. Hou, E. Arenholz, A. T. N' Diaye, A. Tan, K. Uchida, K. Sato, S. Okamoto, Y. Tserkovnyak, Z. Q. Qiu, and E. Saitoh, *Nat. Comm.* **7**, 12670 (2016)
20. O. Mosendz, V. Vlaminck, J. E. Pearson, F. Y. Fradin, G. E. W. Bauer, S. D. Bader, and A. Hoffmann, *Phys. Rev. B* **82**, 214403 (2010).
21. M. Harder, Z. X. Cao, Y. S. Gui, X. L. Fan, and C. -M. Hu, *Phys. Rev. B* **84**, 054423 (2011).
22. M. Obstbaum, M. Härtinger, H. G. Bauer, T. Meier, F. Swientek, C. H. Back, and G. Woltersdorf, *Phys. Rev. B* **89**, 060407(R) (2014).
23. L. Bai, Z. Feng, P. Hyde, H. F. Ding, and C. -M. Hu, *Appl. Phys. Lett.* **102**, 242402 (2013).
24. L. Bai, P. Hyde, Y. S. Gui, C.-M. Hu, V. Vlaminck, J. E. Pearson, S. D. Bader, and A. Hoffmann, *Phys. Rev. Lett.* **111**, 217602 (2013).
25. S. M. Haidar, R. Iguchi, A. Yagmur, J. Lustikova, Y. Shiomi, and E. Saitoh, *J. Appl. Phys.* **117**, 183906 (2015).
26. L. Chen, S. Ikeda, F. Matsukura, and H. Ohno, *Appl. Phys. Exp.* **7**, 013002 (2014).
27. K. Ando, T. Yoshino, and E. Saitoh, *Appl. Phys. Lett.* **94**, 152509 (2009).
28. A. Hoffmann, *IEEE Trans. Mag.* **49**, 5172 (2013).
29. S. S. Mukherjee, P. Deorani, J. H. Kwon, and H. Yang, *Phys. Rev. B* **85**, 094416 (2012).
30. P. Deorani and H. Yang, *Appl. Phys. Lett.* **103**, 232408 (2013).
31. M. Jamali, J. S. Lee, J. S. Jeong, F. Mahfouzi, Y. Lv, Z. Zhao, B. K. Nikolić, K. A. Mkhoyan, N. Samarth, and J. -P. Wang, *Nano Lett.* **15**, 7126 (2015).
32. R. Iguchi, K. Ando, R. Takahashi, T. An, E. Saitoh, and T. Sato, *Jpn. J. Appl. Phys.* **51**, 103004 (2012).
33. M. V. Costache, S. M. Watts, M. Sladkov, C. H. van der Wal, and B. J. van Wees, *Appl. Phys. Lett.* **89**, 232115 (2006).
34. N. Kuhlmann, A. Vogel and G. Meier, *Phys. Rev. B.* **85**, 014410 (2012).
35. Z. Feng, J. Hu, L. Sun, B. You, D. Wu, J. Du, W. Zhang, A. Hu, Y. Yang, D. M. Tang, B. S. Zhang, and H. F. Ding, *Phys. Rev. B* **85**, 214423 (2012).

Figure Caption

- Fig. 1.** Schematic of experimental setup and optical image of respected devices for measurement of (a) AMR voltage, (b) ISHE voltage, and (c) enlarged view of Py strip, where β defines direction of in-plane H_{dc} with respect to central line.
- Fig. 2.** (a) Dc voltages as a function of H_{dc} at $I_{dc} = 0.4$ mA for different frequency of 4-14 GHz (in step size of 1 GHz) at excitation power of 15 dBm. Inset shows linear scaling of voltage with input power (13-18 dBm) (b) Comparative plot of precession angle versus frequency determined by AMR-method and h_{rf} evaluation from microwave power (P_{trans} , P_{input} and P_{ab}).
- Fig 3.** (a) Frequency dependent spectrum of V_{ISHE} as a function of H_{dc} for Pt/Py in step of 1 GHz. Inset shows V_{ISHE} signal at $f = 10$ GHz, solid circles are experimental data and line is Lorentz fit (b) Frequency dependent spin current density (J_S) obtained using AMR measurement and h_{rf} evaluation from microwave power (P_{trans} , P_{input} and P_{ab}).
- Fig.4.** Frequency dependent Θ_{SH} values obtained by AMR measurement and h_{rf} evaluation from microwave power (P_{trans} , P_{input} and P_{ab}). The dashed line represent average Θ_{SH} value.

Fig. 1.

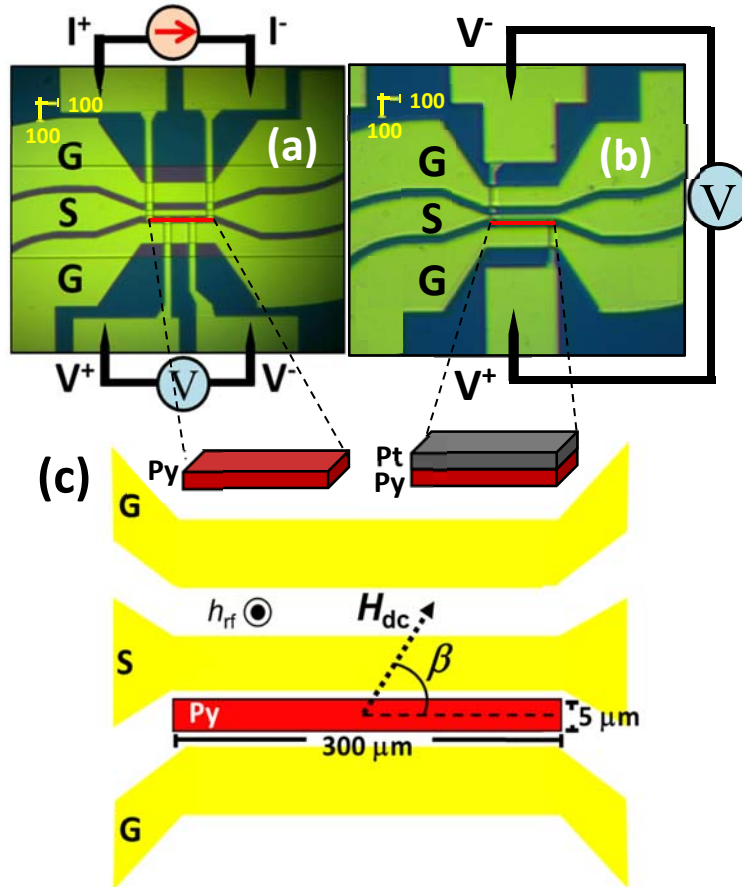


Fig. 2.

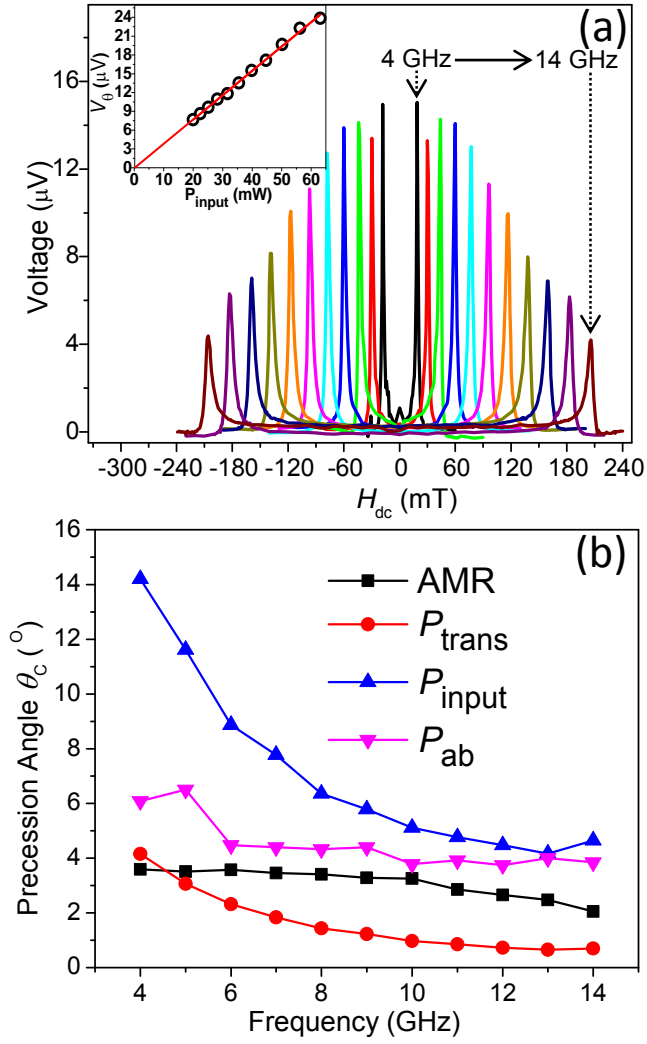


Fig. 3.

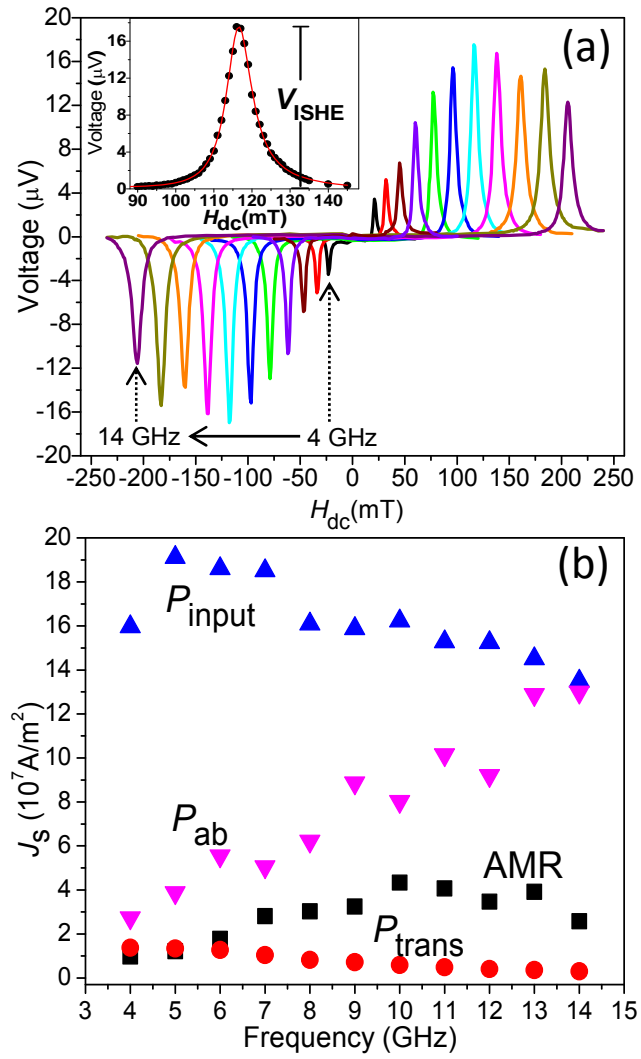
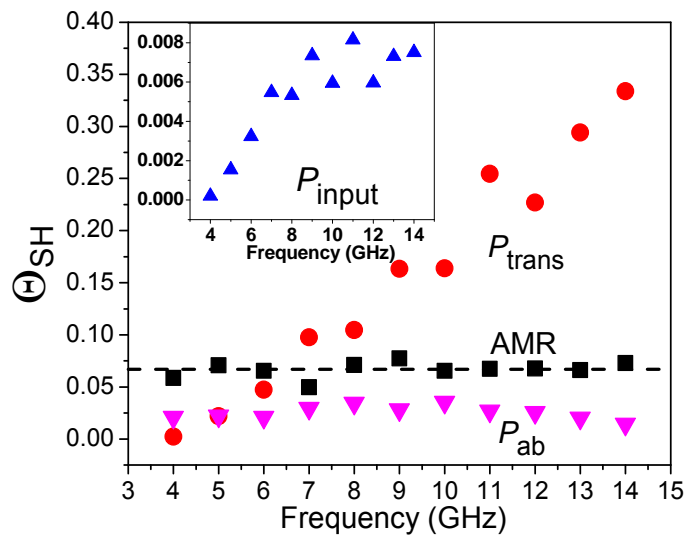


Fig. 4.



Supplementary Material

Microwave transmission intensity (P_{trans}) was measured using power meter (Agilent 53152A) for different applied frequencies, as shown in Fig. S1 (a). The magnetic field h_{rf} applied to the sample was estimated using Ampere's Law, $h_{\text{rf}} = \frac{\mu_0 \sqrt{P_{\text{trans}}/Z}}{2\pi w} \ln\left(1 + \frac{w}{D}\right)$ where w is the width (10 μm) of the signal line in CPW and D is the space (5 μm) between the signal line and the Py micro strip and Z is the characteristic impedance of 50 Ω . On the other hand, microwave absorption intensity (P_{abs}) is estimated from the peak amplitude in the Lorentzian spectra of two-port microwave transmission property $|S_{21}|^2$ measured by the vector network analyzer (Agilent N5222A) as shown in Fig. S1(b).

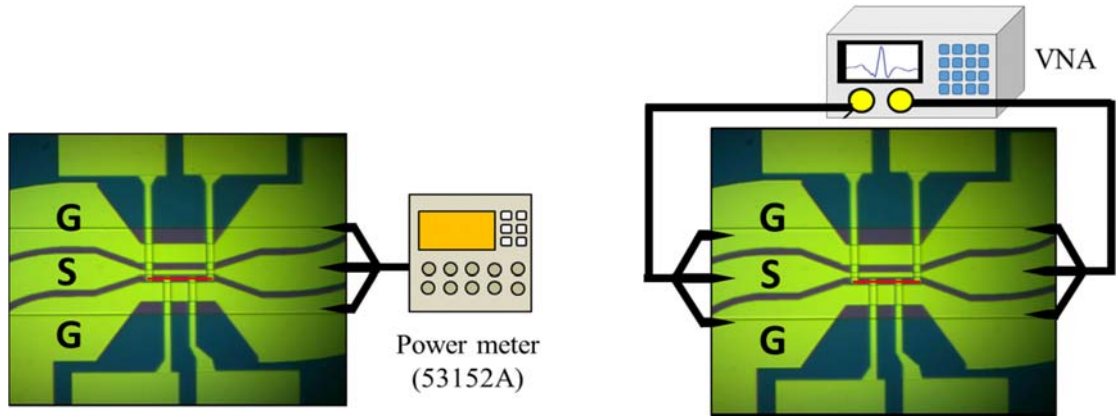


Fig. S1. Schematic for measurement of (a) transmission power P_{trans} and (b) absorption power P_{ab} .

Here $|S_{21}|^2$ denotes the ratio of transmitted microwave power at port 2 to the incident fixed microwave power P_{input} at port 1.^{7, 26} Frequency dependent h_{rf} distribution using P_{ab} can be described as

$$P_{\text{ab}} = \upsilon \times \frac{\mu_0 \gamma M_S}{4\alpha} h_{\text{rf}}^2 \left[\frac{(\gamma M_S + \sqrt{(\gamma M_S)^2 + (2\omega)^2})}{(\gamma M_S)^2 + (2\omega)^2} \right]$$

where υ denotes the volume of the region that is magnetically excited by the microwave in the Py layer and α is the damping constant. Figure S2 depicts the frequency dependent P_{ab} and P_{trans} values which showed different behavior and as a result different Θ_{SH} values are obtained. It is important to mention here that accurate estimation of J_S as well as Θ_{SH} requires accurate value of θ_c . In earlier reports, P_{input} is utilized to determine h_{rf} without taking care of the actual transmission losses in CPW, which leads to overestimated values of θ_c as shown in the present

study. Considering frequency dependent P_{ab} and P_{trans} measurements, we observed different behavior than AMR based results, suggesting that the indirect θ_c measurement techniques provide only a tentative trend.

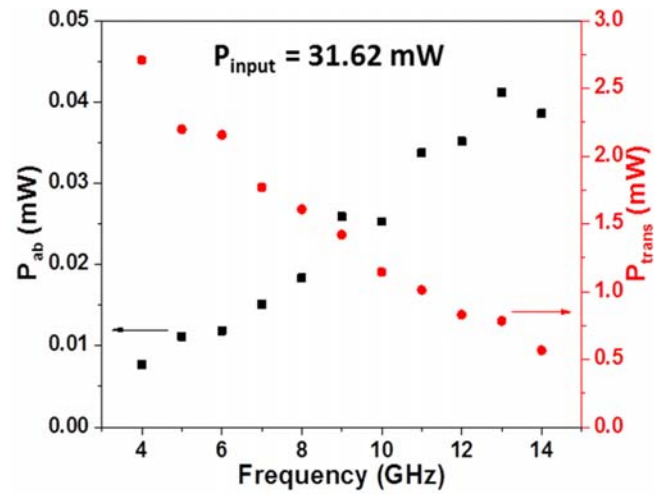


Fig. S2. Frequency dependent of P_{ab} and P_{trans} measured for Py sample